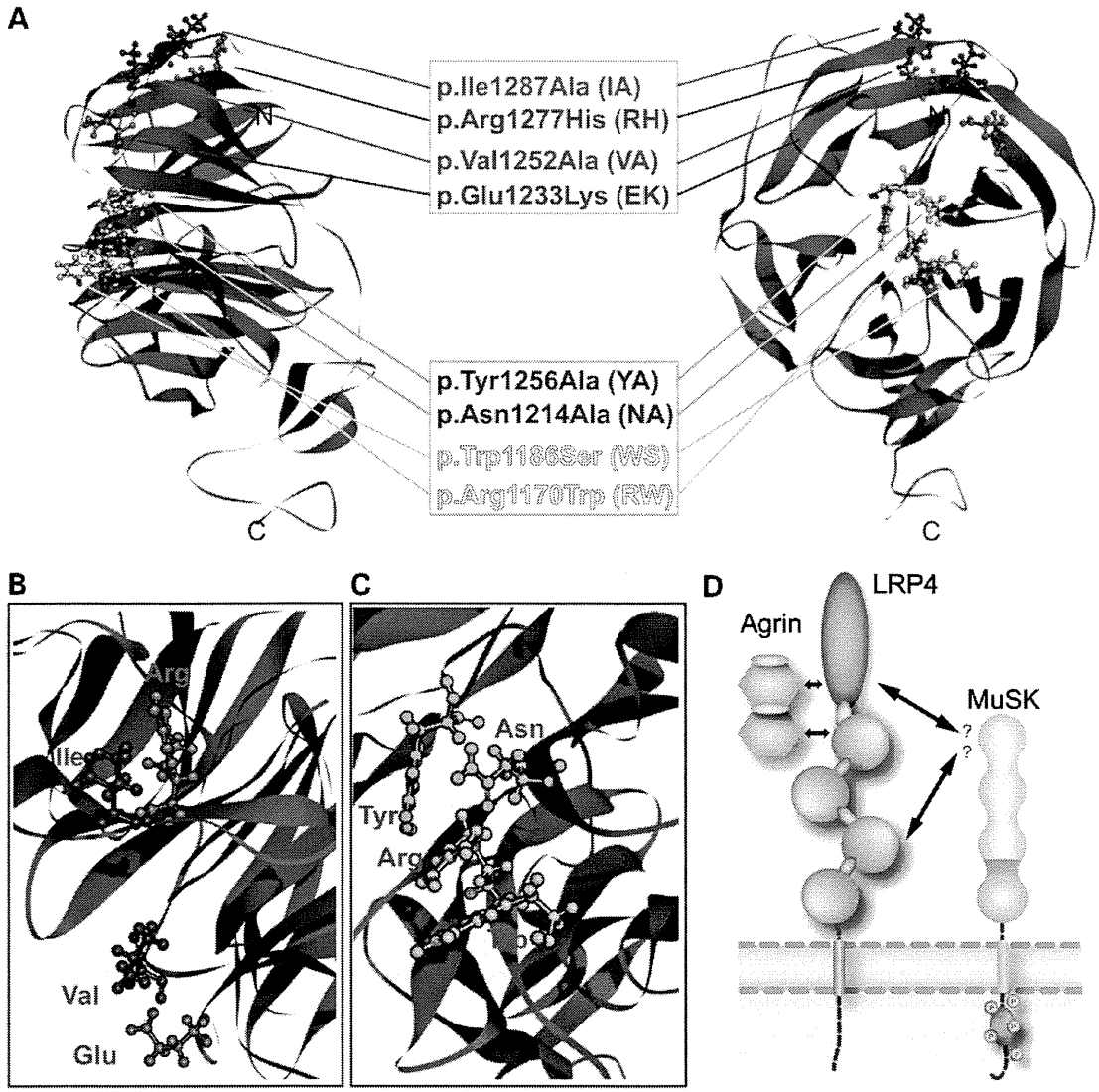

Figure 7. The 3rd β-propeller domain of LRP4 and scheme of agrin/LRP4/MuSK complex. (**A**–**C**) Simulated three-dimensional structure of the 3rd β-propeller domain of LRP4. Positions of the analyzed mutations are indicated. The RH and EK mutations (red) are identified in our CMS patient. The RW and WS mutations (yellow) are reported in sclerosteosis-2 (12). Amino acids that are artificially mutated to alanine are shown in purple or green. Mutations at the edge of the β-propeller domain and in the central cavity are grouped together by boxes. The edge (B) and central cavity (C) of the 3rd β-propeller domain are enlarged to show locations of the naturally occurring and artificially introduced mutations. The viewing positions of (B) and (C) are not identical to (A). (**D**) Scheme of agrin/LRP4/MuSK. Arrows represent direct interactions: Agrin binds to the 1st EGF-like domain and the 1st β-propeller domain of LRP4 (23); MuSK binds to the 4th/5th LDLa repeats and the 3rd β-propeller domain of LRP4 (4). An artificial missense mutation in the 1st IgG-like domain of MuSK impairs binding to LRP4 (4) and deletion of this domain abolishes agrin-mediated AChR clustering (24), but the exact LRP4-binding domain(s) of MuSK remain elusive. We propose that the edge of the 3rd β-propeller domain of LRP4 is essential for binding to MuSK and for signal transduction at NMJ.

fragment in a single direction using ABI SOLiD4 system (Life Technologies). The sequencing fragments were mapped to the human genome hg19/GRCh37 using BioScope 1.4 (Life Technologies). SNVs/indels were called by Avadis NGS 1.3.1 (Agilent) using default parameters. We restricted our analysis to 34 candidate genes that were known to be essential for neuromuscular signal transmission: *ABL2*, *ACHE*, *AGRN*, *APP*, *CHAT*, *CHRNA1*, *CHRNB1*, *CHRND*, *CHRNE*, *CHRNG*, *COLQ*, *CSNK2B*, *DAG1*, *DOK7*, *DTNA*, *DVL1*, *ETV5*, *GFPT1*, *LAMB2*, *LRP4*, *MUSK*, *NRG1*, *NTF4*, *PAK1*, *PGGT1B*, *PHLDB2*, *PLEC*, *RAPSN*, *SCN4A*, *SLC18A3*, *SNTB2*, *STNA1* and *SYNC*.

Primer pairs for each exon and the flanking intron regions of *LRP4* were designed with Primer 3. PCR products were directly sequenced with ABI PRISM 3730 DNA Analyzer and BigDye Terminator Cycle Sequencing Kit version 1.1 according to the manufacturer's protocols (Applied Biosystems).

Plasmids

Full-length human *LRP4* cDNA (Open Biosystems) was cloned into the *Eco*RI site of the pcDNA3.1 mammalian expression vector. The extracellular domain (amino acid 1–1722) of

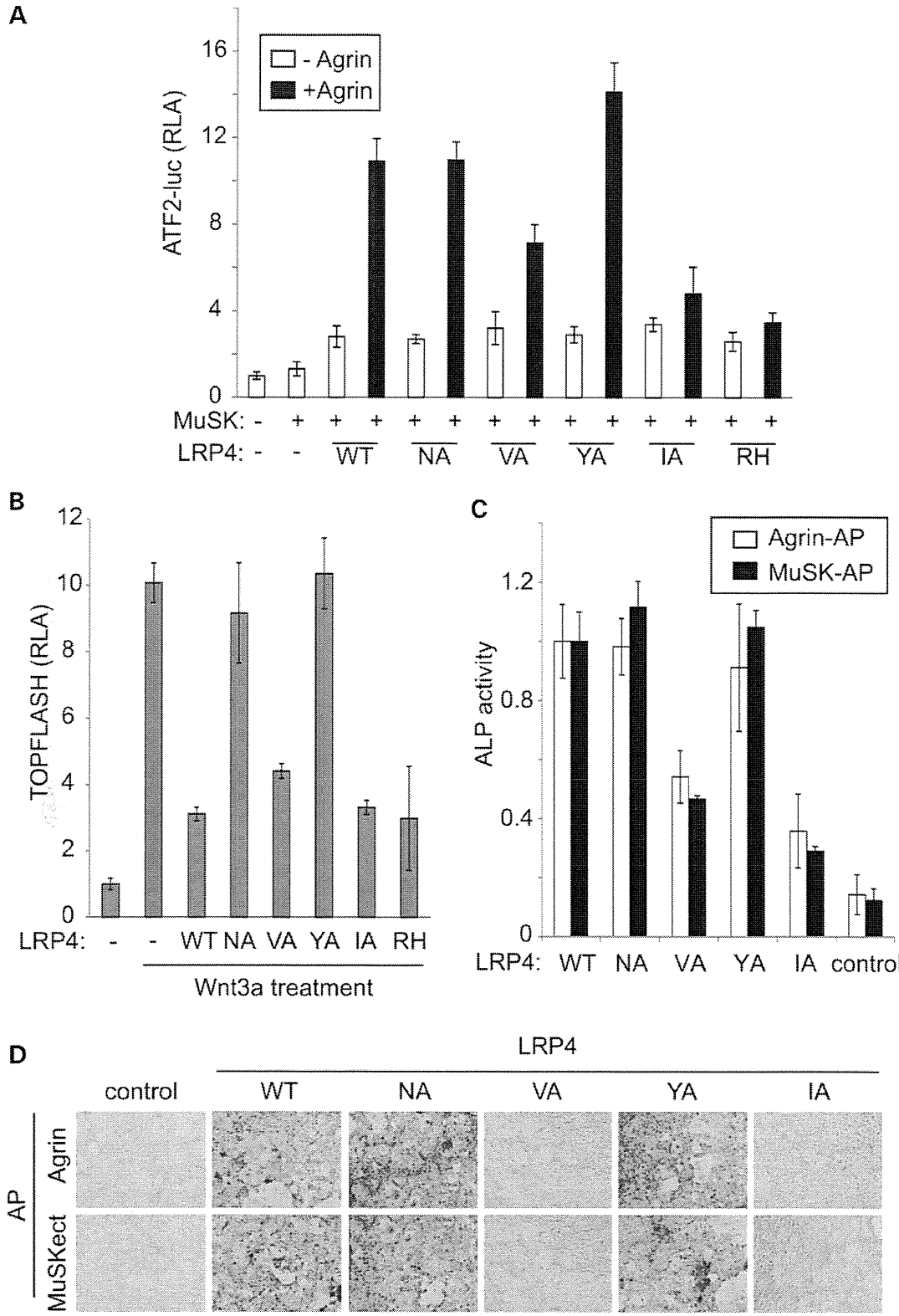

Figure 8. Artificially engineered p.Val1252Ala (VA) and p.Ile1287Ala (IA) compromise agrin-mediated upregulation of MuSK signaling, whereas p.Asn1214Ala (NA) and p.Tyr1256Ala (YA) compromise Wnt-suppressive activity. (**A**) ATF2-luciferase reporter assay of HEK293 cells as in Figs 3A and 6B. The IA and VA mutations are at the edge, whereas the YA and NA mutations are in the central cavity (see Fig. 7A and Supplementary Material, Movie S1). The RH mutation in our CMS patient is included as a control. (**B**) TOPFLASH reporter assay of HEK293 cells as in Figs 3C and 6C. (**C and D**) Cell surface-binding assays as in Figs 5A, B, and 6D. The ALP activities of bound agrin-mycAP and MuSKect-mycAP in three independent wells are shown in (C). Mean and SD are indicated in (A)–(C).

human *LRP4* cDNA was cloned into the *Hin*dIII and *Xba*I sites upstream of a 3xFlag epitope of a mammalian expression vector p3xFlag-CMV-14 to generate hLRP4ecd-Flag for the plate-binding assay. The mouse *Musk* cDNA in pExpress-1 was purchased from Open Biosystems and was used for the luciferase assay in HEK293 cells. Human *MUSK* cDNA with a Flag-tag at the N-terminal end was cloned into the *Eco*RI and *Xba*I sites of the p3xFlag-CMV-14 to generate Flag-MuSK, and was used for the co-immunoprecipitation assay. For vector expressing shRNA against Lrp4, double-stranded oligonucleotides (sense, 5′-GATCCCGGAAGTTTCCTGACATAAATTCAAGAGATTTATGTCAGGAAACTTCCTTTTGGAAA-3′ and 5′-AGCTTTTCCAAAAAGGAAGTTTCCTGACATAAATCTCTTGAATTTATGTCAGGAAACTTCCGG-3′) were cloned into a lentiviral vector pLenti-CMV-GFPx2-DEST, which was kindly provided by Dr Eric Campeau at the University of Massachusetts Medical School. The extracellular domain of mouse *Musk* cDNA fused to a myc-tag and alkaline phosphatase (MuSKect-mycAP) was kindly provided by Dr Lin Mei. To generate rat agrin-mycAP that retains potency to facilitate AChR clustering as a neural agrin, we cloned amino acid 1141–1937 of rat *Agrn* cDNA (M64780.1) into pAPtag-5 (GenHunter) at the *Hin*dIII and *Sna*BI sites, so that the Igk-originated signal peptide is attached upstream of the insert and the myc-tag/alkaline phosphatase downstream. Mutant *LRP4* plasmids carrying p.Arg1170Trp, p.Trp1186Ser, p.Asn1214Ala, p.Glu1233Lys, p.Val1252Ala, p.Tyr1256Ala, p.Arg1277His and p.Ile1287Ala were generated by the QuikChange Site-Directed Mutagenesis kit (Stratagene). Lack of PCR artifacts was verified by sequencing the entire inserts. Super 8x TOPFLASH plasmid (Addgene), ATF2-Luc (21) and phRL-TK Renilla luciferase vector (Promega) were used for the luciferase reporter assay.

Cell cultures

HEK293, L, COS and C2C12 cells were cultured in the Dulbecco's modified Eagle's medium (DMEM) supplemented with 10% fetal calf serum and transfected with FuGENE 6 transfection reagent (Roche). L cells stably expressing Wnt3a were purchased from ATCC. Conditioned media were prepared by culturing Wnt3a-producing and control L cells for 4 days. The LRP4ecd-Flag, agrin-mycAP and MuSKect-mycAP proteins were produced by transfecting each plasmid into HEK293 cells in serum-free DMEM. Recombinant rat C-terminal agrin (10 ng/ml, R&D systems) was used for agrin treatment except for the binding assays. For AChR clustering assay, C2C12 myoblast were seeded on a plate coated with collagen I (BD Biosciences) and differentiated in DMEM supplemented with 2% horse serum for 5 days. The differentiated myotubes were electroporated with shLrp4 and each LRP4 cDNA construct using the NEPA21 electroporator and the CUY900-13-3-5 electrode for attached cells (NepaGene), and then treated with 2 μg/ml doxycycline for 2 days to induce shRNA expression. Cells were treated with 10 ng/ml agrin to induce AChR clusters for 12 h. Cells were stained with 10 mg/ml Axexa594-conjugated α-bungarotoxin (1:100, Invitrogen) to label AChR and fixed in 2% paraformaldehyde. Fluorescence images were observed under an Olympus XL71 fluorescence microscope and analyzed with MetaMorph software (Molecular Devices). The lengths of AChR clusters and myotubes were defined as the longest axes of Alexa594 signals and GFP signals, respectively, in the transfected cells. AChR clusters with the axis length <4 μm were excluded from the analysis.

Luciferase assays

HEK293 cells were transfected with ATF2-Luc and phRL-TK along with the *MUSK* and *LRP4* cDNAs. Cells were cultured for 24 h in the presence or absence of agrin in the medium in a 96-well plate. Cells were lysed with the passive lysis buffer (Promega) and assayed for the luciferase activity using the Dual luciferase system (Promega). Each experiment was done in triplicate.

Biotinylation of LRP4 on plasma membrane and western blotting

HEK293 cells transfected with MuSK and LRP4 plasmids in the presence of agrin were cultured for 24 h. C2C12 myoblasts transfected with shLrp4 and human *LRP4* cDNA using NEPA21 electroporator and electroporation cuvettes (NepaGene) were cultured in a differentiation medium for 2 days in the presence of 2 μg/ml doxycycline and 10 ng/ml agrin. Efficient downregulation of Lrp4 was confirmed by quantitative RT–PCR. Cells were lysed with a buffer containing 50 mM HEPES pH 7.0, 150 mM NaCl, 10% glycerol, 1% Triton X-100, 1.5 mM $MgCl_2$, 1 mM EGTA, 100 mM NaF, 10 mM sodium pyrophosphate, 1 μg/μl aprotinin, 1 μg/μl leupeptin, 1 μg/μl pepstatin A, 1 mM PMSF, 1 mM sodium orthovanadate. Cell lysates were subjected to coimmunoprecipitation using 1 μg of anti-phosphotyrosine antibody (4G10, Upstate) attached to protein G Sepharose beads (GE Healthcare). For biotinylation of LRP4 on plasma membrane, LRP4-transfected HEK293 cells were washed twice with PBS containing 1 mM $MgCl_2$ and 0.1 mM $CaCl_2$ (PBS/CM), followed by incubation with 0.5 mg/ml sulfo-NHS-SS-biotin (Pierce) in PBS/CM at room temperature for 30 min. The cells were then washed once with PBS/CM and incubated with 10 mM monoethanolamine for quenching free biotin. The cells were harvested with RIPA buffer (Pierce) after several washing with ice-cold PBS and the cell lysates were incubated with streptavidin sepharose beads (GE healthcare) to purify cell membrane protein. Total or precipitated proteins were dissolved in 1 × laemmli buffer, separated on a 10 or 7.5% SDS–polyacrylamide gel and transferred to a polyvinylidene fluoride membrane (Immobilon-P, Millipore). Membranes were washed in Tris-buffered saline containing 0.05% Tween 20 (TBS-T) and blocked for 1 h at room temperature in TBS-T with 3% bovine serum albumin. The membranes were incubated overnight at 4°C either with the mouse monoclonal anti-Myc 9E10 (dilution 1:500, sc-40, Santa Cruz Biotechnology), anti-Flag M2 (dilution 1:4000, F1804, Sigma-Aldrich), anti-LRP4 (dilution 1:1000, ab85697, Abcam), anti-MuSK (1:500, sc-6009, Santa Cruz Biotechnology) or anti-β-actin (dilution 1:200, sc-47778, Santa Cruz Biotechnology) antibody. The membranes were washed three times for 10 min with TBS-T and incubated with secondary goat anti-mouse IgG antibody conjugated to horseradish peroxidase (HRP) (1:6000, LNA931 V/AG, GE Healthcare) for 1 h at room temperature. The blots were detected with Amersham ECL western blotting detection reagents (GE Healthcare) and quantified with the ImageJ program.

Preparation of agrin-MycAP, MuSKect-MycAP and LRP4ecd-flag proteins

Agrin-mycAP and MuSKect-mycAP in the conditioned media of transfected HEK293 cells were concentrated ~100-fold using Amicon Ultra-4 filters (Millipore). For the cell surface-binding assay, we used the concentrated conditioned media. For the plate-binding assay, we further purified agrin-mycAP and MuSKect-mycAP using the c-myc-Tagged Protein Mild Purification Kit ver. 2 (MBL). Wild-type and mutant hLRP4ecd-Flag proteins were purified with the Anti-DYKDDDDK-tag Antibody Beads (Wako) from the conditioned medium of the transfected HEK293. Purified MuSKect-mycAP and hLRP4ecd-Flag were detected by anti-myc antibody (9E10, Abcam) or anti-Flag antibody (M2, Sigma-Aldrich), respectively. We also measured concentrations of each protein by SDS–PAGE followed by protein staining with SYBRO Ruby Protein Gel Stain (Molecular Probes) using BSA as a standard.

Cell surface- and plate-binding assays

For the cell surface-binding assay, COS cells were transfected with LRP4 using FuGENE 6 (Roche). Cells were incubated 24 h with concentrated conditioned medium containing either agrin-mycAP or MuSKect-mycAP for 1.5 h at RT. Cells were washed with HABH buffer (0.5 mg/ml bovine serum albumin, 0.1% NaN_3 and 20 mM HEPES, pH 7.0, in Hank's balanced salt solution), fixed in 60% acetone for 10 min on ice followed by 4% paraformaldehyde in 20 mM HEPES (pH 7.0) in Hank's balanced salt solution for 10 min on ice. Fixed cells were washed once with 20 mM HEPES (pH 7.0) and 150 mM NaCl, incubated at 65°C for 30 min, washed with 0.1 M Tris–HCl (pH 8.0), washed with water and stained with NBP/BCIP solution (Roche). For plate-biding assay, the Immuno plate (Nunc) was coated with 0.15 μg of purified wild-type or mutant LRP4ecd-Flag at 4°C overnight and then incubated with a blocking buffer (1%BSA in PBS) at RT for 1 h. For the binding assays, 80 μl of serially diluted agrin-mycAP or MuSKect-mycAP were added to wells that were coated with wild-type or mutant LRP4ecd-Flag in a blocking buffer. The reagents were incubated for 2 h at RT, and then washed twice with PBS. Bound AP activity was measured using LabAssay ALP (Wako).

Homology modeling

The primary sequence of the 3rd β-propeller domain of hLRP4 (accession number: AAI36669, amino acid 1048–1350) and the coordinates of crystal structure of the 1st β-propeller domain (amino acid 20–326) of human LRP6 (PDB ID: 3SOV) were loaded into the Molecular Operating Environment software (MOE, Chemical Computing Group). The primary structures of each β-propeller domain of hLRP4 and hLRP6 were sequence-aligned and manually corrected by the structure–alignment method. Molecular mechanics were calculated by an MMFF94x force field.

SUPPLEMENTARY MATERIAL

Supplementary Material is available at *HMG* online.

ACKNOWLEDGEMENTS

We thank Keiko Itano for expert technical assistance.

Conflict of Interest statement. None declared.

FUNDING

This work was supported by Grants-in-Aid from the MEXT and MHLW of Japan to B.O., M.I., A.M. and K.O.; and by NIH Research Grant NS6277 from the NINDS and by Research Grant from the MDA to A.G.E.

REFERENCES

1. Engel, A.G. (2012) Current status of the congenital myasthenic syndromes. *Neuromuscul. Disord.*, **22**, 99–111.
2. Kim, N., Stiegler, A.L., Cameron, T.O., Hallock, P.T., Gomez, A.M., Huang, J.H., Hubbard, S.R., Dustin, M.L. and Burden, S.J. (2008) Lrp4 is a receptor for agrin and forms a complex with MuSK. *Cell*, **135**, 334–342.
3. Zhang, B., Luo, S., Wang, Q., Suzuki, T., Xiong, W.C. and Mei, L. (2008) LRP4 serves as a coreceptor of agrin. *Neuron*, **60**, 285–297.
4. Zhang, W., Coldefy, A.S., Hubbard, S.R. and Burden, S.J. (2011) Agrin binds to the N-terminal region of Lrp4 protein and stimulates association between Lrp4 and the first immunoglobulin-like domain in muscle-specific kinase (MuSK). *J. Biol. Chem.*, **286**, 40624–40630.
5. Wu, H., Xiong, W.C. and Mei, L. (2010) To build a synapse: signaling pathways in neuromuscular junction assembly. *Development*, **137**, 1017–1033.
6. Yumoto, N., Kim, N. and Burden, S.J. (2012) Lrp4 is a retrograde signal for presynaptic differentiation at neuromuscular synapses. *Nature*, **489**, 438–442.
7. Wu, H., Lu, Y., Shen, C., Patel, N., Gan, L., Xiong, W.C. and Mei, L. (2012) Distinct roles of muscle and motoneuron LRP4 in neuromuscular junction formation. *Neuron*, **75**, 94–107.
8. Higuchi, O., Hamuro, J., Motomura, M. and Yamanashi, Y. (2011) Autoantibodies to low-density lipoprotein receptor-related protein 4 in myasthenia gravis. *Ann. Neurol.*, **69**, 418–422.
9. Zhang, B., Tzartos, J.S., Belimezi, M., Ragheb, S., Bealmear, B., Lewis, R.A., Xiong, W.C., Lisak, R.P., Tzartos, S.J. and Mei, L. (2012) Autoantibodies to lipoprotein-related protein 4 in patients with double-seronegative myasthenia gravis. *Arch. Neurol.*, **69**, 445–451.
10. Pevzner, A., Schoser, B., Peters, K., Cosma, N.C., Karakatsani, A., Schalke, B., Melms, A. and Kroger, S. (2012) Anti-LRP4 autoantibodies in AChR- and MuSK-antibody-negative myasthenia gravis. *J. Neurol.*, **259**, 427–435.
11. Li, Y., Pawlik, B., Elcioglu, N., Aglan, M., Kayserili, H., Yigit, G., Percin, F., Goodman, F., Nurnberg, G., Cenani, A. *et al.* (2010) LRP4 mutations alter Wnt/beta-catenin signaling and cause limb and kidney malformations in Cenani–Lenz syndrome. *Am. J. Hum. Genet.*, **86**, 696–706.
12. Leupin, O., Piters, E., Halleux, C., Hu, S., Kramer, I., Morvan, F., Bouwmeester, T., Schirle, M., Bueno-Lozano, M., Fuentes, F.J. *et al.* (2011) Bone overgrowth-associated mutations in the LRP4 gene impair sclerostin facilitator function. *J. Biol. Chem.*, **286**, 19489–19500.
13. Styrkarsdottir, U., Halldorsson, B.V., Gretarsdottir, S., Gudbjartsson, D.F., Walters, G.B., Ingvarsson, T., Jonsdottir, T., Saemundsdottir, J., Snorradottir, S., Center, J.R. *et al.* (2009) New sequence variants associated with bone mineral density. *Nat. Genet.*, **41**, 15–17.
14. Choi, H.Y., Dieckmann, M., Herz, J. and Niemeier, A. (2009) Lrp4, a novel receptor for Dickkopf 1 and sclerostin, is expressed by osteoblasts and regulates bone growth and turnover in vivo. *PLoS ONE*, **4**, e7930.
15. Johnson, E.B., Steffen, D.J., Lynch, K.W. and Herz, J. (2006) Defective splicing of Megf7/Lrp4, a regulator of distal limb development, in autosomal recessive mulefoot disease. *Genomics*, **88**, 600–609.
16. Johnson, E.B., Hammer, R.E. and Herz, J. (2005) Abnormal development of the apical ectodermal ridge and polysyndactyly in Megf7-deficient mice. *Hum. Mol. Genet.*, **14**, 3523–3538.
17. Rasi, S., Spina, V., Bruscaggin, A., Vaisitti, T., Tripodo, C., Forconi, F., De Paoli, L., Fangazio, M., Sozzi, E., Cencini, E. *et al.* (2011) A variant of the LRP4 gene affects the risk of chronic lymphocytic leukaemia transformation to Richter syndrome. *Br. J. Haematol.*, **152**, 284–294.

18. Adzhubei, I.A., Schmidt, S., Peshkin, L., Ramensky, V.E., Gerasimova, A., Bork, P., Kondrashov, A.S. and Sunyaev, S.R. (2010) A method and server for predicting damaging missense mutations. *Nat. Methods*, **7**, 248–249.
19. Kumar, P., Henikoff, S. and Ng, P.C. (2009) Predicting the effects of coding non-synonymous variants on protein function using the SIFT algorithm. *Nat. Protoc.*, **4**, 1073–1081.
20. Schwarz, J.M., Rodelsperger, C., Schuelke, M. and Seelow, D. (2010) MutationTaster evaluates disease-causing potential of sequence alterations. *Nat. Methods*, **7**, 575–576.
21. Ohkawara, B. and Niehrs, C. (2011) An ATF2-based luciferase reporter to monitor non-canonical Wnt signaling in Xenopus embryos. *Dev. Dyn.*, **240**, 188–194.
22. Okada, K., Inoue, A., Okada, M., Murata, Y., Kakuta, S., Jigami, T., Kubo, S., Shiraishi, H., Eguchi, K., Motomura, M. *et al.* (2006) The muscle protein Dok-7 is essential for neuromuscular synaptogenesis. *Science*, **312**, 1802–1805.
23. Zong, Y., Zhang, B., Gu, S., Lee, K., Zhou, J., Yao, G., Figueiredo, D., Perry, K., Mei, L. and Jin, R. (2012) Structural basis of agrin-LRP4-MuSK signaling. *Genes. Dev.*, **26**, 247–258.
24. Zhou, H., Glass, D.J., Yancopoulos, G.D. and Sanes, J.R. (1999) Distinct domains of MuSK mediate its abilities to induce and to associate with postsynaptic specializations. *J. Cell Biol.*, **146**, 1133–1146.
25. Huze, C., Bauche, S., Richard, P., Chevessier, F., Goillot, E., Gaudon, K., Ben Ammar, A., Chaboud, A., Grosjean, I., Lecuyer, H.A. *et al.* (2009) Identification of an agrin mutation that causes congenital myasthenia and affects synapse function. *Am. J. Hum. Genet.*, **85**, 155–167.
26. Chevessier, F., Faraut, B., Ravel-Chapuis, A., Richard, P., Gaudon, K., Bauche, S., Prioleau, C., Herbst, R., Goillot, E., Ioos, C. *et al.* (2004) MUSK, a new target for mutations causing congenital myasthenic syndrome. *Hum. Mol. Genet.*, **13**, 3229–3240.
27. Selcen, D., Fukuda, T., Shen, X.-M. and Engel, A.G. (2004) Are MuSK antibodies the primary cause of myasthenic symptoms? *Neurology*, **62**, 1945–1950.
28. Shiraishi, H., Motomura, M., Yoshimura, T., Fukudome, T., Fukuda, T., Nakao, Y., Tsujihata, M., Vincent, A. and Eguchi, K. (2005) Acetylcholine receptors loss and postsynaptic damage in MuSK antibody-positive myasthenia gravis. *Ann. Neurol.*, **57**, 289–293.
29. Punga, A.R., Maj, M., Lin, S., Meinen, S. and Ruegg, M.A. (2011) MuSK levels differ between adult skeletal muscles and influence postsynaptic plasticity. *Eur. J. Neurosci.*, **33**, 890–898.
30. Bao, J., Zheng, J.J. and Wu, D. (2012) The structural basis of DKK-mediated inhibition of Wnt/LRP signaling. *Sci. Signal*, **5**, pe22.
31. Karner, C.M., Dietrich, M.F., Johnson, E.B., Kappesser, N., Tennert, C., Percin, F., Wollnik, B., Carroll, T.J. and Herz, J. (2010) Lrp4 regulates initiation of ureteric budding and is crucial for kidney formation–a mouse model for Cenani-Lenz syndrome. *PLoS ONE*, **5**, e10418.
32. Glinka, A., Wu, W., Delius, H., Monaghan, A.P., Blumenstock, C. and Niehrs, C. (1998) Dickkopf-1 is a member of a new family of secreted proteins and functions in head induction. *Nature*, **391**, 357–362.
33. Semenov, M., Tamai, K. and He, X. (2005) SOST is a ligand for LRP5/LRP6 and a Wnt signaling inhibitor. *J. Biol. Chem.*, **280**, 26770–26775.
34. Lu, Y., Tian, Q.B., Endo, S. and Suzuki, T. (2007) A role for LRP4 in neuronal cell viability is related to apoE-binding. *Brain Res.*, **1177**, 19–28.
35. Ohazama, A., Johnson, E.B., Ota, M.S., Choi, H.Y., Porntaveetus, T., Oommen, S., Itoh, N., Eto, K., Gritli-Linde, A., Herz, J. *et al.* (2008) Lrp4 modulates extracellular integration of cell signaling pathways in development. *PLoS ONE*, **3**, e4092.
36. Fambrough, D.M., Engel, A.G. and Rosenberry, T.L. (1982) Acetylcholinesterase of human erythrocytes and neuromuscular junctions: homologies revealed by monoclonal antibodies. *Proc. Natl. Acad. Sci. USA*, **79**, 1078–1082.
37. Gautron, J. (1974) Cytochimie ultrastructurale des acétylcholinestérases. *Microscopie*, **21**, 259–264.
38. Engel, A.G. (2004) In Engel, A.G. and Franzini-Armstrong, C. (eds.), *Myology*. 3rd edn. McGraw Hill, New York, Vol. I, pp. 681–690.
39. Engel, A.G. (1994) In Engel, A.G. and Franzini-Armstrong, C. (eds.), *Myology*. 2nd edn. McGraw-Hill, New York, Vol. 2, pp. 1018–1045.
40. Engel, A.G., Lindstrom, J.M., Lambert, E.H. and Lennon, V.A. (1977) Ultrastructural localization of the acetylcholine receptor in myasthenia gravis and in its experimental autoimmune model. *Neurology*, **27**, 307–315.
41. Engel, A.G., Nagel, A., Walls, T.J., Harper, C.M. and Waisburg, H.A. (1993) Congenital myasthenic syndromes: I. Deficiency and short open-time of the acetylcholine receptor. *Muscle Nerve*, **16**, 1284–1292.
42. Uchitel, O., Engel, A.G., Walls, T.J., Nagel, A., Atassi, M.Z. and Bril, V. (1993) Congenital myasthenic syndromes: II. Syndrome attributed to abnormal interaction of acetylcholine with its receptor. *Muscle Nerve*, **16**, 1293–1301.
43. Milone, M., Hutchinson, D.O. and Engel, A.G. (1994) Patch-clamp analysis of the properties of acetylcholine receptor channels at the normal human endplate. *Muscle Nerve*, **17**, 1364–1369.
44. Shen, X.M., Brengman, J.M., Sine, S.M. and Engel, A.G. (2012) Myasthenic syndrome AChRalpha C-loop mutant disrupts initiation of channel gating. *J. Clin. Invest.*, **122**, 2613–2621.

genesis 52:56-67 (2014)

TECHNOLOGY REPORT

SIP1 Expression Patterns in Brain Investigated by Generating a SIP1-EGFP Reporter Knock-in Mouse

Yuriko Nishizaki, Tsuyoshi Takagi, Fumiko Matsui, and Yujiro Higashi*

Department of Perinatology, Institute for Developmental Research, Aichi Human Service Center, Kasugai, Aichi, Japan

Received 7 June 2013; Revised 23 October 2013; Accepted 8 November 2013

Summary: A loss of function of SIP1 (Smad interacting protein 1) in the mouse as well as in human of Mowat-Wilson syndrome results in severe and multiple defects in neural tissue development, especially in the brain. However, no detailed expression analysis of SIP1 during brain development has been previously reported. In this study, we describe the generation of an EGFP knock-in reporter mouse for the *Sip1* locus and our subsequent analysis of SIP1-EGFP fusion protein expression during brain development. SIP1-EGFP expression was observed in the pyramidal neurons of the hippocampus, the dentate gyrus, and the postmitotic neurons in the cerebral cortex. In layer 5 of the cerebral cortex, SIP1-EGFP expression was complementary to the Ctip2-expressing neurons, most of which are thought to be the corticospinal neurons. This suggested that SIP1-EGFP expressing cells might have the specific trajectory targets other than the spinal region. We further observed SIP1-EGFP expression in oligodendrocytes of the corpus callosum and fimbria, Bergmann glial cells of the cerebellum, the olfactory bulb, and in the serotonergic and dopaminergic neurons of the raphe nuclei in the brainstem. These findings may help to clarify the unknown roles of SIP1 in these cells and the pathoetiology of Mowat-Wilson syndrome. genesis 52:56–67, 2014. © 2013 Wiley Periodicals, Inc.

Key words: zeb2; zfhx1b; Mowat-Wilson syndrome

RESULTS AND DISCUSSION

Smad-interacting-protein 1 (Sip1, also called Zeb2/Zfhx1b) is the causative gene for Mowat-Wilson syndrome (Wakamatsu *et al.*, 2001) and encodes a transcription factor containing two-zinc finger clusters and a homeodomain-like sequence (Verschueren *et al.*, 1999). SIP1 interacts with the TGF-β superfamily signaling regulator, Smads (Verschueren *et al.*, 1999) and thereby regulates the expression of the downstream genes (van Grunsven *et al.*, 2003). *Sip1* is expressed in the developing neural tube, the neural crest cells, the hippocampus, and the cerebral cortex (Miyoshi *et al.*, 2006; Van de Putte *et al.*, 2003). *Sip1*-deficient mice show defects of the open neural tube, delamination arrest of the neural crest cells (Van de Putte *et al.*, 2003), hypo-cellularity of the enteric neurons, which may be a possible cause of Hirschsprung disease found in some Mowat-Wilson syndrome patients (Van de Putte *et al.*, 2007), a lack of hippocampus and corpus callosum structures (Miquelajauregui *et al.*, 2007), and abnormalities in cerebrocortical lamination (Seuntjens *et al.*, 2009). Recently, it has also been reported that *Sip1* plays important roles in myelination of the central nervous system (Weng *et al.*, 2012), and in migration of the cortical interneurons (McKinsey *et al.*, 2013; van den Berghe *et al.*, 2013). However, no detailed analysis of SIP1 expression has been previously carried out and the data that does exist is insufficient to determine the functional role of SIP1 in the brain. Although the expression analysis using polyclonal antibody for SIP1 is a straightforward method, the results depend on source of the antibody and the polypeptide sequence against which was raised and the experimental protocols and techniques. Experimental tools to detect the SIP1 protein expression sensitively and reproducibly *in vivo* are therefore needed.

* Correspondence to: Yujiro Higashi, Department of Perinatology, Institute for Developmental Research, Aichi Human Service Center, 713-8 Kagiya-cho, Kasugai, Aichi 480-0392, Japan.
E-mail: higashi@inst-hsc.jp

Contract grant sponsor: KAKENHI, JSPS, Contract grant number: 23791215; Contract grant sponsor: Takeda Science Foundation
Published online 17 November 2013 in
Wiley Online Library (wileyonlinelibrary.com).
DOI: 10.1002/dvg.22726

In this study, we report the generation of an enhanced green fluorescent protein (EGFP) knock-in reporter mouse in which the *Sip1* locus was subjected to gene targeted recombination. We then describe the detailed analysis of the SIP1 expression profile in the brain during development. The expression of the SIP1-EGFP fusion protein could be evaluated in this system by direct detection of green fluorescence in living mice or by staining of fixed tissues with GFP antibodies. Through this analysis, SIP1 expression was very clearly observed not only in the hippocampus and cerebral cortex (Cx), but also in the oligodendrocytes of the corpus callosum and fimbria, the olfactory bulb (Ob), the Bergmann glial cells (BG) of the cerebellum, and the raphe nucleus of the brainstem. These findings have not been previously reported.

By use of a gene targeting strategy (Fig. 1a), we generated a SIP1-EGFP knock-in reporter mouse (we designate the knock-in allele as $Sip1^{SIP1\text{-}EGFP}$ hereafter) harboring an in-frame SIP1-EGFP fusion protein in place of the authentic SIP1 protein at the endogenous *Sip1* locus. This animal enabled us to not only use EGFP as a reporter, but also to trace the subcellular localization of SIP1 protein to further understand its functional role. Two out of 192 ES clones were confirmed as the correct homologs recombinants (Fig. 1b). The germ-line chimeras produced from these two independent clones were then mated to the Cre recombinase expressing mouse line (Zp3-cre) to delete the neo cassette element, thereby finally obtaining $Sip1^{SIP1\text{-}EGFP/+}$ mice.

EGFP fluorescence of unfixed SIP1-EGFP embryos or brains was detectable (Fig. 1c and data not shown). To undertake more detailed analysis, we performed immunohistochemistry of $Sip1^{SIP1\text{-}EGFP/+}$ mice with anti-GFP antibodies. Gross observations of whole brain tissues revealed that SIP1-EGFP was expressed in the periventricular zones, cortical plate, and subpallium at embryonic day 13.5 (E13.5; Fig. 1e,f, E13); Ob, hippocampus and periventricular area at E16.5 (Fig. 1h,i, E16); and ganglionic eminence (GE), thalamic region, colliculus, and cerebellum at postnatal day 0 (P0; Fig. 1k,l). Those expressions were in good accordance with the *Sip1* mRNA expressing pattern (Fig. 1d,e,g,h,j,k, Miquelajauregui *et al.*, 2007; Seuntjens *et al.*, 2009).

A marked expression of SIP1-EGFP was detected in the cortical plate (CP) at E13.5 (Fig. 2a). Ctip2 is expressed strongly in layer 5 and weakly in layer 6 (McKenna *et al.*, 2011). By double staining for GFP and Ctip2, it was further observed that the most pial population of SIP1-EGFP expressing cells also expressed Ctip2 (Fig. 2a-c). At E16.5, SIP1-EGFP was found to be widely expressed in the entire CP (Fig. 2d). A cell population that expressed only SIP1-EGFP (i.e., not Ctip2) appeared in the upper layer (Fig. 2f). In the middle area of the CP, the cells expressing only Ctip2 (i.e., not SIP1-EGFP) were observed (Fig. 2e,f). At around P0, SIP1-EGFP- and Ctip2-double-positive cells were observed in the cells of prospective layer 6 with smaller nuclei [Fig. 2g-i, m-o, (McKenna *et al.*, 2011)]. At layer 5, we observed that the number of SIP1-EGFP- and Ctip2-double-positive cells became lower and that of single-positive cells increased as development progressed (Fig. 2i,l,o). Ctip2 is expressed in cortico-spinal neurons (CSNs) but not in callosal neurons in layer 5 (Arlotta *et al.*, 2005), suggesting that SIP1-expressing cells are not CSNs, but could form part of the callosal neurons.

In the hippocampus of the $Sip1^{SIP1\text{-}EGFP/+}$ mice, strong expression of SIP1-EGFP was observed throughout the developmental and adult stages (Fig. 3a,e,h). SIP1-EGFP was detected in the cornu ammonis (CA)1, CA2, CA3 of the hippocampus and dentate gyrus (DG) (Fig. 3). At P10, whilst Sox2 expression was detected in the cells around the DG, SIP1-EGFP positive cells in DG did not express Sox2 (Fig. 3d), indicating that SIP1-expressing cells in DG are postmitotic granule cells. At the adult stages, SIP1-EGFP expressing cells also expressed the neuronal marker NeuN (Fig. 3h-j). These results reveal that SIP1-expressing cells in the hippocampus are pyramidal neurons.

Around the hippocampus of adult $Sip1^{SIP1\text{-}EGFP/+}$ mice, we observed tandemly lined SIP1-EGFP positive cells with small nuclei in the fimbria (Fig. 3h and arrowheads in Fig. 3k). The expression of APC, a marker for oligodendrocytes (Bhat *et al.*, 1996), was observed in SIP1-EGFP positive cells in the fimbria of 16-week-old (16 week) adult mice (Fig. 3k-m), suggesting that these cells are oligodendrocytes. Similar cells (closely apposed and double-positive for APC and SIP1-EGFP) were also found in the corpus callosum (data not shown). It has been reported that SIP1 is expressed in the oligodendrocytes of the mouse spinal cord, and is required for myelination in the central nervous system (Weng *et al.*, 2012).

In the Ob, SIP1-EGFP expressing cells were detectable throughout the lifetime (Figs. 1h,k and 4a-c). SIP1-EGFP was expressed in the periglomerular layer (PGL), granule cell layer (GCL) and mitral cell layer (MCL) (Fig. 4a-f). SIP1-EGFP expression was observed also in the ventricular and subventricular zone of the lateral ventricle (LV) (Fig. 4a,i) and the rostral migratory stream (RMS) toward the Ob (Fig. 4a). RMS is composed of the Tbr1/2-positive neuroblasts (Brill *et al.*, 2009) and surrounding GFAP-positive glial tube cells (Doetsch *et al.*, 1997). Both of those cell types expressed SIP1-EGFP (Fig. 4g,h). This is compatible with the phenotype of the RMS of Sip1-conditional-knockout mice in the neocortex (Nityanandam *et al.*, 2012).

In the cerebellum of the 8 week adult $Sip1^{SIP1\text{-}EGFP/+}$ mice, SIP1-EGFP expressing cells were evident at the border between the molecular and granular layers (Fig. 5a) and expressed BG marker Sox2 (Sottile *et al.*, 2006) (Fig. 5a-c) extending their processes to the molecular layer (Fig. 5d,d′,e,e′). SIP1-EGFP expressing cells were

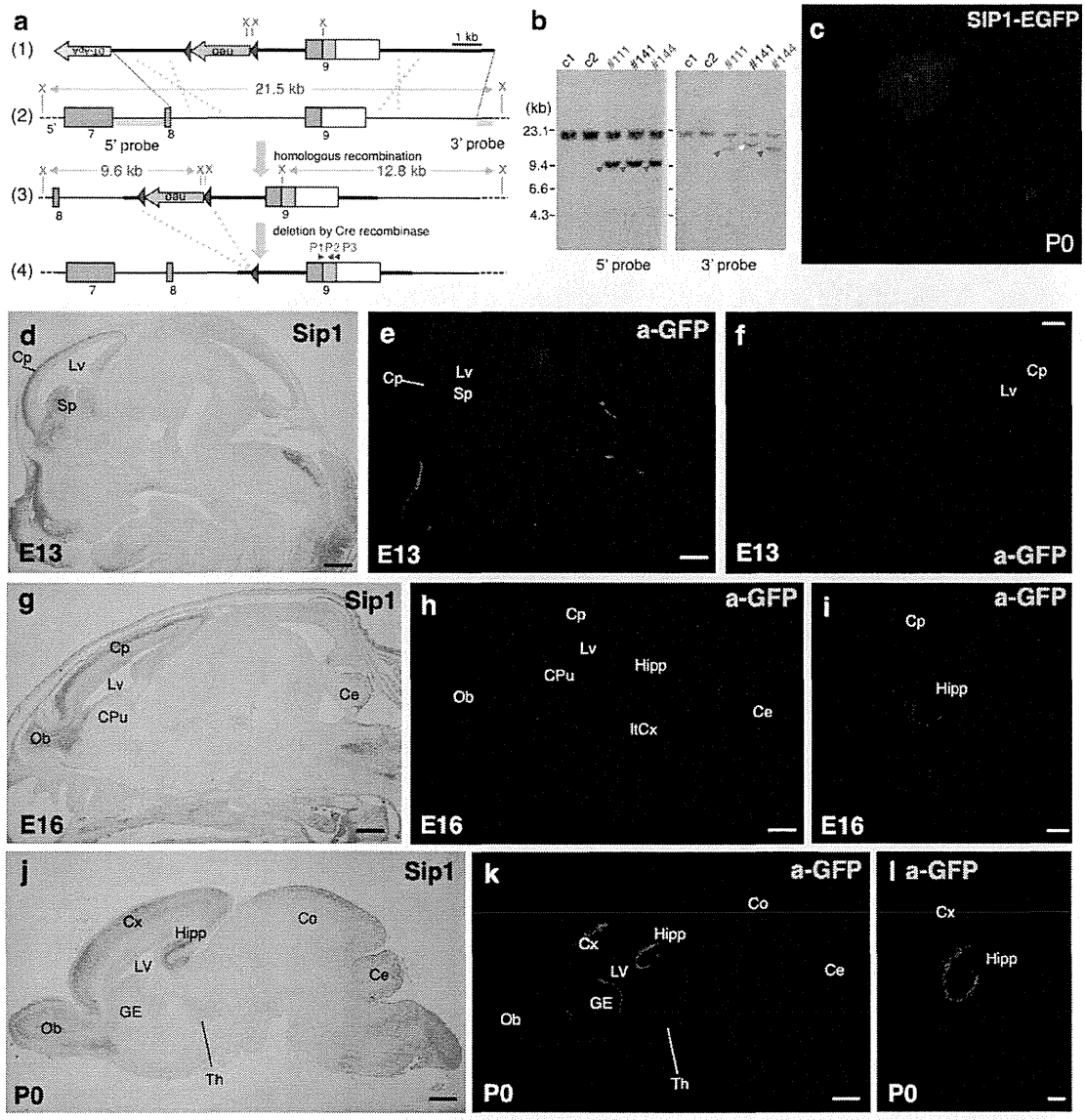

FIG. 1. Generation of *Sip1*$^{SIP1\text{-}EGFP/+}$ knock-in reporter mice and overview of the SIP1-EGFP reporter expression profile in the mouse brain. (**a**) The strategy used to generate the *Sip1*$^{SIP1\text{-}EGFP}$ knock-in allele by gene targeting. The targeting vector encodes EGFP (green box) fused to the SIP1 protein carboxy terminus. The loxP-flanked neomycin (neo) selection cassette introduced into intron 8 was eventually removed by Cre recombinase. The XbaI (X) sites and the expected length of the extra bands on a Southern blot that correspond to the desired homologs recombination are denoted by the red letters and lines. The 5′ and 3′ external probes are indicated by transparent gray bars. The light blue and open boxes denote the *Sip1* coding and noncoding exons, respectively. The dark blue triangles indicate loxP sequences. The triangles (designated P1, P2, and P3) indicate the primers used for genotyping of the *Sip1*$^{SIP1\text{-}EGFP}$ allele. (**b**) Southern blot hybridization analysis of the ES clones. Using the 5′ probe (left) clones #111, #141, and #144 showed an expected additional band of 9.6 kb (red arrowhead). When using the 3′ probe (right panel), clones #111 and #144 showed a band of the expected length of 12.8 kb (red arrowheads) but the clone #141 did not (white arrowhead). C1 and C2 are non-targeted control clones. (**c**) Unfixed brain from a *Sip1*$^{SIP1\text{-}EGFP/+}$ mouse at P0 exposed to excitation light. Anterior is to the left. The anterior areas including the cerebral cortex fluoresced strongly when illuminated with blue light. (**d–l**) Images showing the *in situ* hybridization results with *Sip1* antisense mRNA probe on sagittal sections of the wild-type embryo or neonatal mice at E13.5 (d), E16.5 (g), P0 (j), and the immunohistochemical staining results with an anti-GFP antibody on sagittal (e, h, k) or coronal (f, i, l) sections of the *Sip1*$^{SIP1\text{-}EGFP}$ mice at E13.5 (e, f), E16.5 (h, i), P0 (k, l). Anterior is to the left. At E13.5, *Sip1* mRNA and SIP1-EGFP expression was observed in the cortical plate, and subpallium (d, e). Almost all the expression sites of SIP1-EGFP corresponded to the *Sip1* mRNA expression sites. By immunostaining detection, the SIP1-EGFP expression in periventricular areas was remarkable (e), while the signals detected by *in situ* hybridization seem to be weaker (d) than protein detection. At E16.5, *Sip1* mRNA and SIP1-EGFP expression was observed in the cortical plate (Cp), hippocampus (Hipp), periventricular areas, olfactory bulb (Ob), and lobe tip of the cortex (ltCx) (g, h, i). At P0, the expression of *Sip1* mRNA and SIP1-EGFP was detected in the cerebral cortex (Cx), hippocampus (Hipp), periventricular area, and olfactory bulb (Ob) (j, k, l). The expressions were also observed in the thalamic region (Th), cerebellum (Ce), and ganglionic eminence (GE) at P0 (j, k). Scale bars, 500 μm in d, e, g, h, j, k, 200 μm in f, i, l. Ce, cerebellum; Co, colliculus; Cp, cortical plate; CPu, caudate-putamen; Cx, cerebral cortex; Hipp, hippocampus; ltCx, lobe tip of the cortex; Lv, lateral ventricle; GE, ganglionic eminence; Ob, olfactory bulb; Th, thalamus; Sp, subpallium.

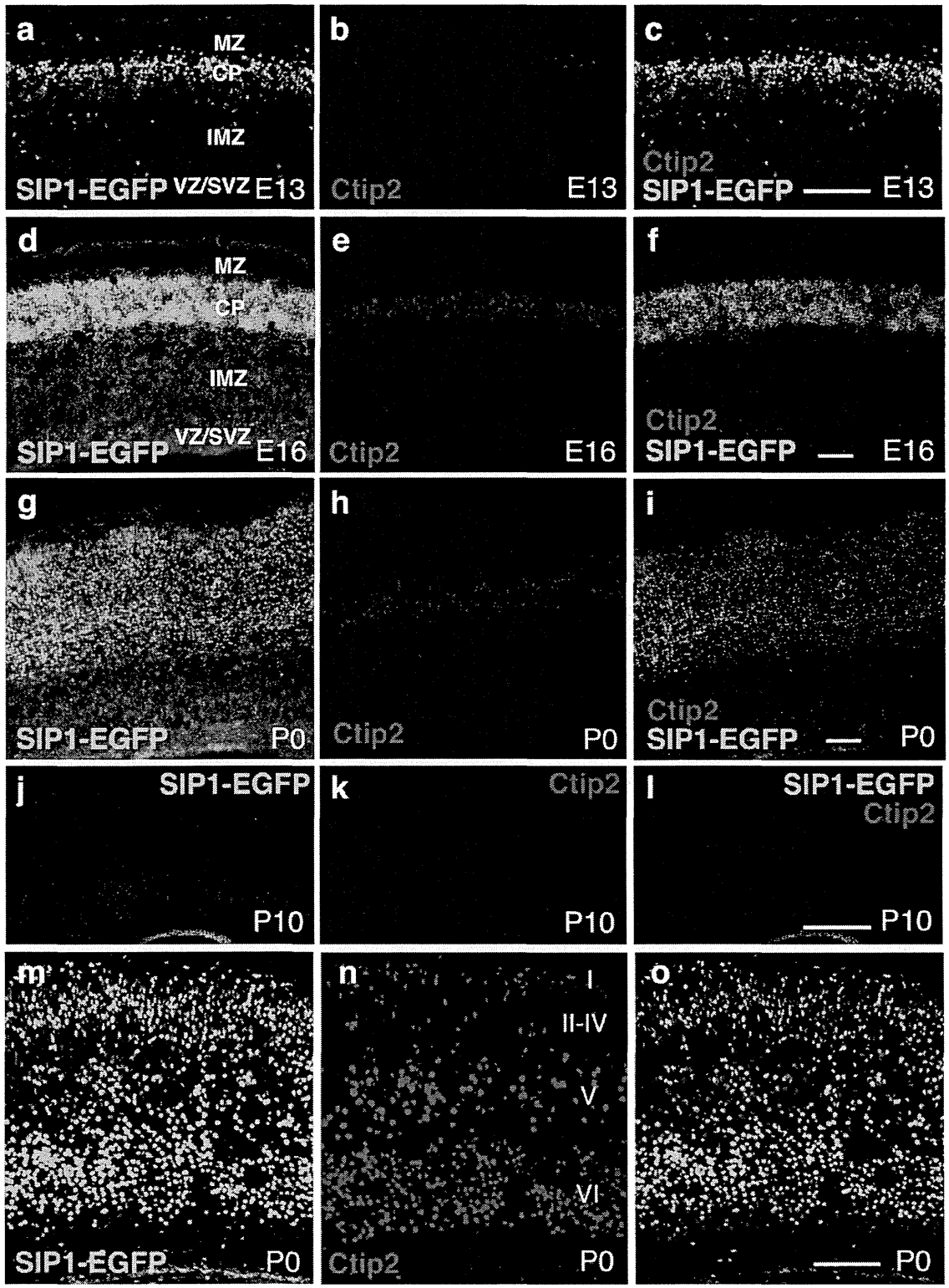
a
MZ
CP
IMZ
SIP1-EGFP VZ/SVZ E13
b
Ctip2 E13
c
Ctip2
SIP1-EGFP E13
d
MZ
CP
IMZ
SIP1-EGFP VZ/SVZ E16
e
Ctip2 E16
f
Ctip2
SIP1-EGFP E16
g
SIP1-EGFP P0
h
Ctip2 P0
i
Ctip2
SIP1-EGFP P0
j
SIP1-EGFP
P10
k
Ctip2
P10
l
SIP1-EGFP
Ctip2
P10
m
SIP1-EGFP P0
n
I
II-IV
V
VI
Ctip2 P0
o
P0

Fig. 2.

found to express neither the Purkinje cell (PC) marker calbindin (Hatten *et al.*, 1997), nor the golgi cell marker MGLUR2 (Ohishi *et al.*, 1993) (Fig. 5g,h). At the earlier stage, the SIP1-EGFP expressing cells also expressed Sox2 (Fig. 5f) and they were found to be a distinct population from the calbindin positive PC progenitors (Fig. 5i). It has been reported that the BG is associated with granule cells in the developing cerebellum and with PC in the adult cerebellum (Yamada and Watanabe, 2002). Clarifying the role of SIP1 in the differentiation and function of BG would contribute significantly to our understanding of the pathology of Mowat-Wilson syndrome.

In the brainstems of the P0 $Sip1^{SIP1\text{-}EGFP/+}$ mice, SIP1-EGFP expressions were found in the cellular nuclei among the serotonin-positive cells such as the dorsal raphe nucleus (DRN) (Fig. 6a-f), and both the Median and Para-Median Raphe nucleus (MnR and PMnR) (Fig. 6g-i). SIP1-EGFP expressing cells were also evident among some of the cells in the tyrosine hydroxylase (TH)-positive Caudal Linear nucleus of the raphe (CLi) (Fig.6 g-i). The expression and function of SIP1 in serotonergic or dopaminergic neurons in mammals has not been reported to date. Recently, it has been demonstrated that the SIP1 homolog in the sea urchin is required for the differentiation of serotonergic neurons in the embryo (Yaguchi *et al.*, 2012), suggesting that SIP1 may also play this important roles in mammals.

In this study, we characterize the SIP1 expression pattern in the mouse brain, using a $Sip1^{SIP1\text{-}EGFP}$ knock-in reporter mouse developed in our laboratory. A common feature of the SIP1-expressing regions that were revealed in our analysis such as the periventricular area (Figs. 1e,f,h,k and 4a,g,i), GE (Fig. 1k) and BG (Fig. 5) is that they are all potential neurogenic sites, where the Sox2 expressions frequently overlapped. The SIP1 expression was also observed in more differentiated and non Sox2-expressing cells such as the cases of the SIP1-positive cells in the Cx, oligodendrocytes, DG, serotonergic, and dopaminergic neurons, suggesting that SIP1 may have much wider roles in the differentiation and/or function of these cells. Our $Sip1^{SIP1\text{-}EGFP/+}$ mouse will also provide a useful research tool to further analyze and elucidate the role of Sip1 in the future.

MATERIALS AND METHODS

Establishment of a SIP1-EGFP Knock-in Mouse Strain

The $Sip1^{SIP1\text{-}EGFP}$ allele was generated by homologs recombination in mouse embryonic stem (ES) cells using a standard gene-targeting protocol as described in our previous report (Higashi *et al.*, 2002). The mouse 129Sv/J genomic DNA BAC clone BAC 312o9 (Nelles *et al.*, 2003) containing the whole *Sip1* gene region was used to construct the targeting vector. A *Sip1* genomic fragment of about 10 kb and covering the region from intron 8-6 kb downstream of the stop codon in exon 9 was subcloned into an MC1-DTApA cassette (Yanagawa *et al.*, 1999) using the recombineering method (Liu *et al.*, 2003). This generated the MC1-DTApA-gSIP1-10kb plasmid.

To generate the SIP1-EGFP fusion protein, we introduced the EGFP coding sequence into the carboxy terminus of the protein coding sequence in a SIP1 expression vector (mSIP1/pcDNA3.1). The termination codon (TAG) was changed to Ser (TAA) followed by an additional 8 extra amino acids derived from the linker sequence of pEGFP-N1 (BD Bioscience Clontech, Mountain View, CA). After verifying the fluorescence activity levels of this construct in cultured cells, the 3′ untranslated region (UTR) of SIP1 of ~1 kb was introduced just downstream of the stop codon of the EGFP protein, thereby forming the chimeric SIP1-EGFP coding-SIP1 3′UTR plasmid. A BamH1-PmlI fragment, a unique fragment within this chimeric plasmid that incorporates a

FIG. 2. Expression of SIP1-EGFP in the cerebral cortex. Immunostained sections of the $Sip1^{SIP1\text{-}EGFP/+}$ mouse brain with anti-GFP antibody (a, d, g, j, m), anti-Ctip2 antibody (b, e, h, k, n), and merged images of these immunostaining results (c, f, i, l, o) at E13.5 (a–c), E16.5 (d–f), P0 (g–i, m–o), and P10 (j–l). Before image merging, the window/level values of the image sources were adjusted to provide a clear discrimination between the double (SIP1-EGFP and Ctip2)-positive and single-positive cells. a–l are sagittal sections; m–o are coronal sections; a–f are sectioned areas of the brain with skin; g–o are isolated brain. (**a–c**) At E13.5, strong expression of SIP1-EGFP can be observed in the cortical plate (CP). In the ventricular/subventricular zone (VZ/SVZ), broad and weak expression of SIP1-EGFP is also observed (a). A few cells strongly expressing SIP1-EGFP were also found in the intermediate zone (IMZ) (a). The most pial population of SIP1-EGFP expressing cells was also found to express Ctip2, a marker for layer 5 and 6 (c). (**d–f**) At E16.5 when cortical plate development is in progress, SIP1-EGFP expression was observed widely in the entire CP (d). Ctip2 expression was observed in the cells with larger nuclei of prospective layer 5 and in the cells with smaller nuclei of prospective layer 6 (e). A SIP1-EGFP single positive population of cells was observed in the upper layer at this stage (green signals in f). In the deep layer of the CP, SIP1-EGFP- and Ctip2-double-positive cells were also observed also at this stage (yellow signals in f). In the middle area of the CP, cells expressing only Ctip2 (negative for SIP1-EGFP) can be observed (red signals in f). (**g–l**) After birth, the SIP1-EGFP expression level in the cerebral cortex appears to be gradually decreased (g, j). Ctip2 expression was observed in the cells with larger nuclei of prospective layer 5 strongly and in the cells with smaller nuclei of prospective layer 6 weakly (h, k). In layer 5, the number of Ctip2-positive cells seems to be increased (red signals in i, l) and that of SIP1-EGFP- and Ctip2-double-positive cells seems to be lowered (yellow signals in i, l) as development progresses. (**m–o**) Immunostained coronal section of the $Sip1^{SIP1\text{-}EGFP/+}$ brain with anti-GFP (m) and anti-Ctip2 (n) antibodies at P0, photographed at a higher magnification. SIP1-EGFP expression could be observed in the entire layer of the cerebral cortex (m). Ctip2 expressing cells in layer 5 with large nuclei and in layer 6 with small nuclei were observed (n); the image in (o) is a merged image of (m) and (n). MZ, marginal zone; CP, cortical plate; IMZ, intermediate zone; VZ, ventricular zone; SVZ, subventricular zone. Scale bars, 100 μm (a–i, m–o); 500 μm (j–l).

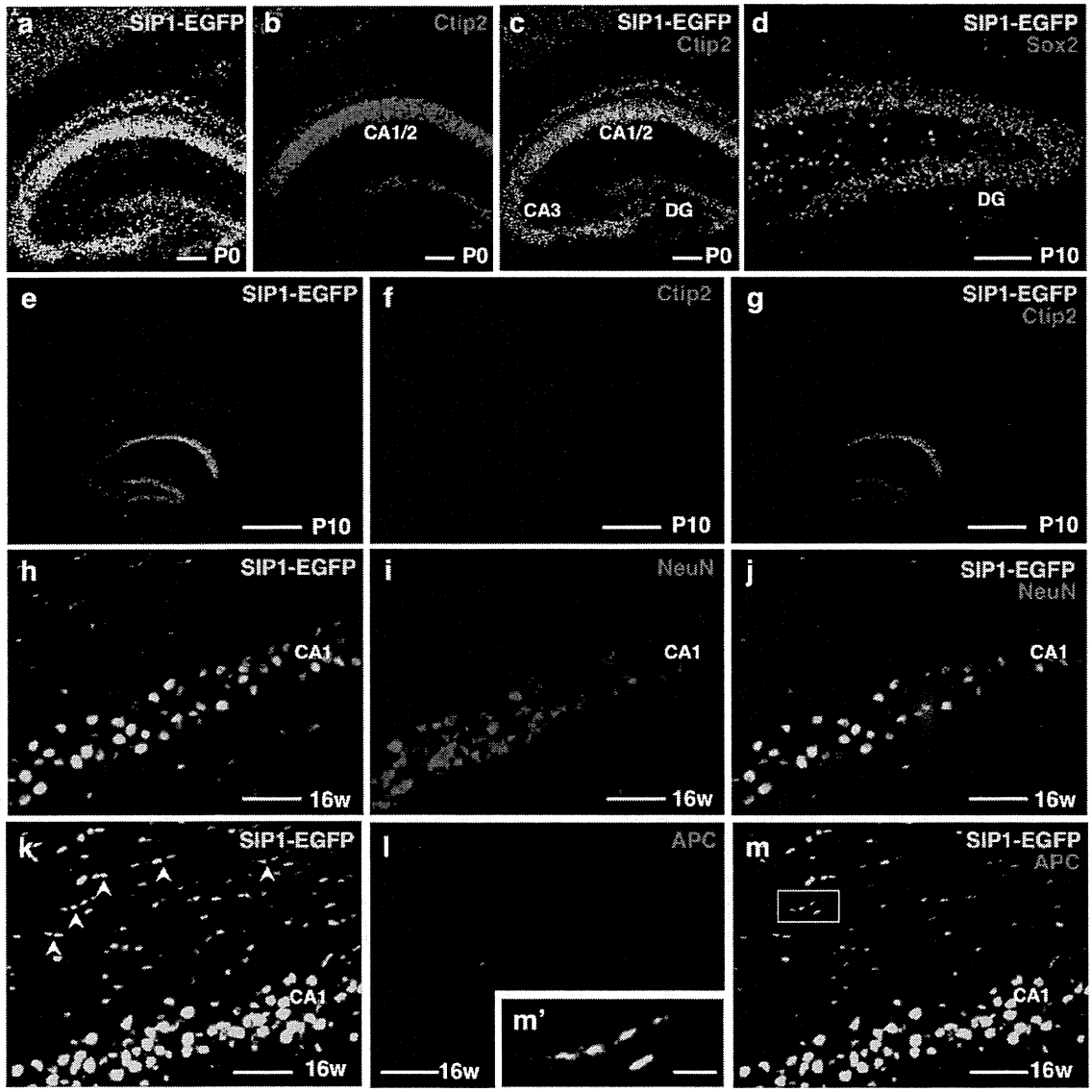

FIG. 3. Expression of SIP1-EGFP in the hippocampus, dentate gyrus, and oligodendrocytes. (**a–c**) Immunostained coronal section of the P0 *Sip1*$^{SIP1\text{-}EGFP/+}$ mouse brain with anti-GFP (green signal in a) and anti-Ctip2 (red signal in b) antibodies. (c) is a merged image of (a) and (b). SIP1-EGFP expression was observed in CA1, CA2, CA3, and the dentate gyrus (a). Ctip2 expression was observed in CA1, CA2, and dentate glanule cells (b). Almost all of the SIP1-EGFP positive cells in CA1 expressed Ctip2. In the dentate gyrus, SIP1-EGFP expression was more widely observed than Ctip2 (c). (**d**) Double immunostained sagittal section of the P10 *Sip1*$^{SIP1\text{-}EGFP/+}$ mouse brain with an anti-GFP antibody (green) and anti-Sox2 antibody (red). Sox2-expressing cells were detected around the dentate gyrus and were found to be distinctly different from the cells that express SIP1-EGFP, indicating that SIP1-EGFP expressing cells in the dentate gyrus are postmitotic granule cells. (**e–g**) Sagittal section of the P10 *Sip1*$^{SIP1\text{-}EGFP/+}$ mouse brain immunostained with anti-GFP (e) and anti-Ctip2 (f) antibody. (g) is a merged image of (e) and (f). Before image merging, the window/level values of the image sources were adjusted to enable a clear discrimination between the double- and single-positive cells. Continuous expression of SIP1-EGFP was observed in the hippocampus and dentate gyrus after birth. (**h–j**) Coronal section of the hippocampus from a 16-week-old (16w) *Sip1*$^{SIP1\text{-}EGFP/+}$ mouse brain immunostained with anti-GFP (h) and anti-NeuN (i) antibodies. (j) is a merged image of (h) and (i). The window/level values of the image sources were optimized for image merging. SIP1-EGFP positive cells in CA1 were also found to express NeuN, indicating that SIP1-expressing cells in the hippocampus are pyramidal neurons. CA, cornu ammonis; DG, dentate gyrus. Bars, 100 μm (a–d), 500 μm (e–g), and 50 μm (h–j). (**k–m**) Expression of SIP1-EGFP in oligodendrocytes. Coronal sections of the hippocampus of a 16w *Sip1*$^{SIP1\text{-}EGFP/+}$ mouse brain were immunostained with anti-GFP (green in k) and anti-adenomatous polyposis coli (APC) (red in l) antibodies. (m) is a merged image of (k) and (l). SIP1-EGFP expression could be observed in tandemly lined interfascicular oligodendrocytes of the fimbriae with small nuclei along the nerve fascicles in the area surrounding the hippocampus (arrowheads in k). The SIP1-EGFP positive cells also expressed APC, a marker for oligodendrocytes (m, m′). SIP1-EGFP and APC expression was observed in the nucleus and cytoplasm, respectively, of the oligodendrocytes [m′, a higher magnification image of the rectangular region in (m)]. Scale bars: 50 μm (k–m); 10 μm (m′).

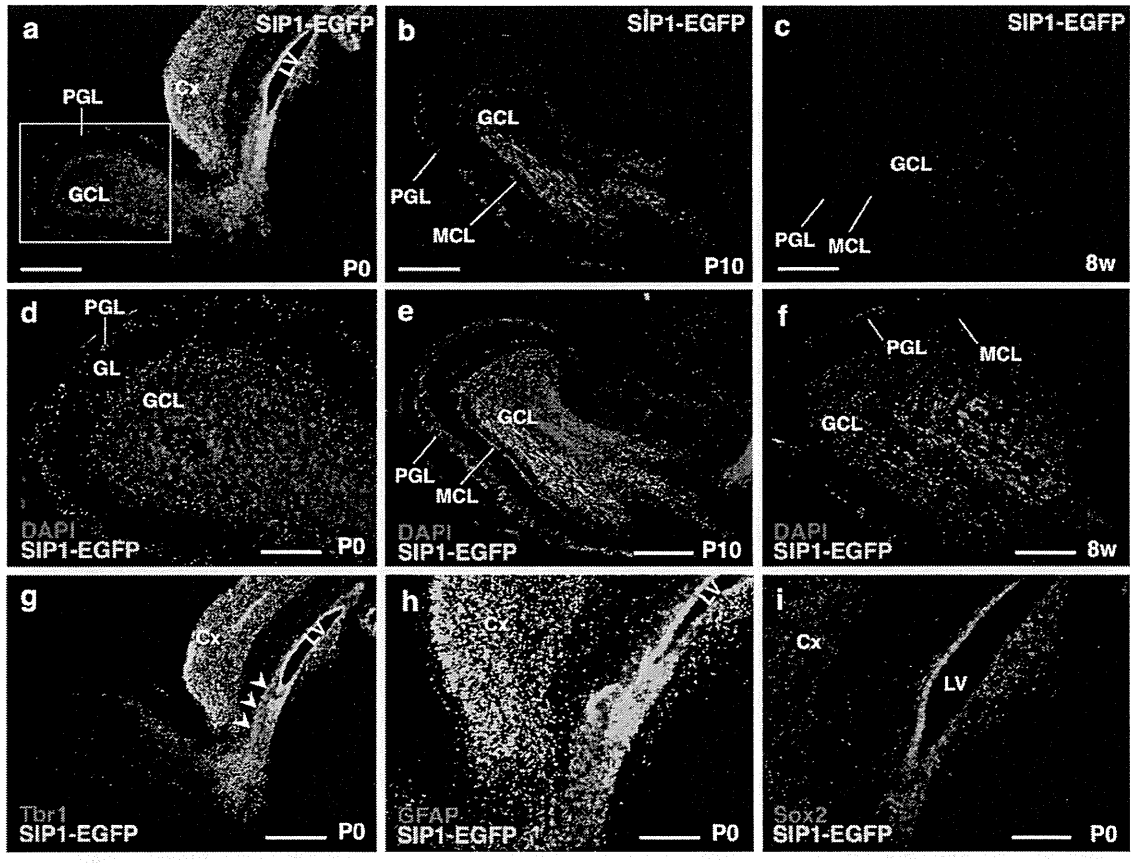

FIG. 4. Expression of SIP1-EGFP in the olfactory bulb. (**a–f**) Immunostained sagittal sections of the *Sip1*$^{SIP1\text{-}EGFP/+}$ mouse brain around the olfactory bulb. (a) and (d) are sections at P0. (a) is a low-magnification image of anti-GFP antibody staining. (d) is a high-magnification image of a rectangular region of (a) and double-stained with anti-GFP antibody (green) and DAPI (blue). SIP1-EGFP expressing cells could be observed in the periglomerular layer (PGL) and granule cell layer (GCL) of the olfactory bulb. (b) and (e) are immunostained sections with anti-GFP antibody at P10. (e) is a double-stained image of (b) with anti-GFP antibody (green) and DAPI (blue). SIP1-EGFP expression was observed in the developed structures of the olfactory bulb. Also at this stage, many cells in the periglomerular layer (PGL), granule cell layer (GCL), and mitral cell layer (MCL) of the olfactory bulb expressed SIP1-EGFP. (c) and (f) are immunostained sections with anti-GFP antibody at 8 week. (f) is a double-stained image of (c) with anti-GFP antibody (green) and DAPI (blue). The continued expression of SIP1-EGFP was observed in periglomerular layer (PGL), granule cell layer (GCL), and mitral cell layer (MCL) of the olfactory bulb also at adult stage. (**g–i**) Immunostained sagittal sections of the *Sip1*$^{SIP1\text{-}EGFP/+}$ mouse brain around the olfactory bulb at P0. (g) is a double-stained image with anti-GFP (green) and Tbr1 (red) antibodies. (h) is a higher-magnification image around the rostral migratory stream stained with anti-GFP (green) and GFAP (red) antibodies. (i) is a higher-magnification around lateral ventricle (LV) of the same section of (a), double-stained image with anti-GFP (green) and Sox2 (red) antibodies. A dorsal population of the SIP1-EGFP expressing cells expressed Tbr1, a marker for neuroblast cells of the rostral migratory stream from dorsal subventricular zone (SVZ) of the lateral ventricle (LV) toward the olfactory bulb (arrowheads in g). A portion of SIP1-expressing cells in the rostral migratory stream also expressed GFAP, a marker for glial tube cells, which guide the neuroblasts migration (h). The ventricular zone of the lateral ventricle (LV) expressed both SIP1-EGFP and Sox2. On the other hand, the cells detached from the ventricular zone alternately expressed SIP1-EGFP or Sox2. SIP1-EGFP and Sox2 double-positive cells were hardly found in the rostral migratory stream (i). MCL, mitral cell layer; GCL, granule cell layer; PGL, periglomerular layer; GL, glomerular layer; LV, lateral ventricle; Cx, cerebral cortex. Scale bars, 500 μm (a, b, c, e, f, g), 200 μm (d, h, i).

part of SIP1 exon 9, the EGFP coding region and a part of the 3′ UTR, was used to replace the endogenous BamH1-PmlI fragment of the MC1-DTApA-gSIP1-10kb plasmid yielding the MC1-DTApA-gSIP1-EGFP-10kb plasmid. Finally, the neomycin cassette flanked by the loxP sequence from the pGPS21loxFRTNeo vector (Aoyama *et al.*, 2005) was amplified by PCR and introduced into intron 8 at ~1 kb upstream of exon 9 in the MC1-DTApA-gSIP1-EGFP-10kb plasmid via the recombineering method thus generating the final targeting vector plasmid (Fig. 1a).

R1 ES cells (Nagy *et al.*, 1993) were transformed by electroporation with the linearized targeting vector plasmid, followed by G418 selection. The ES cell colonies were then screened for homologs recombination by Southern blotting hybridization against 5′ and 3′ external probes (the positions of these probes are indicated in Fig. 1a). Among the 192 clones examined, 2

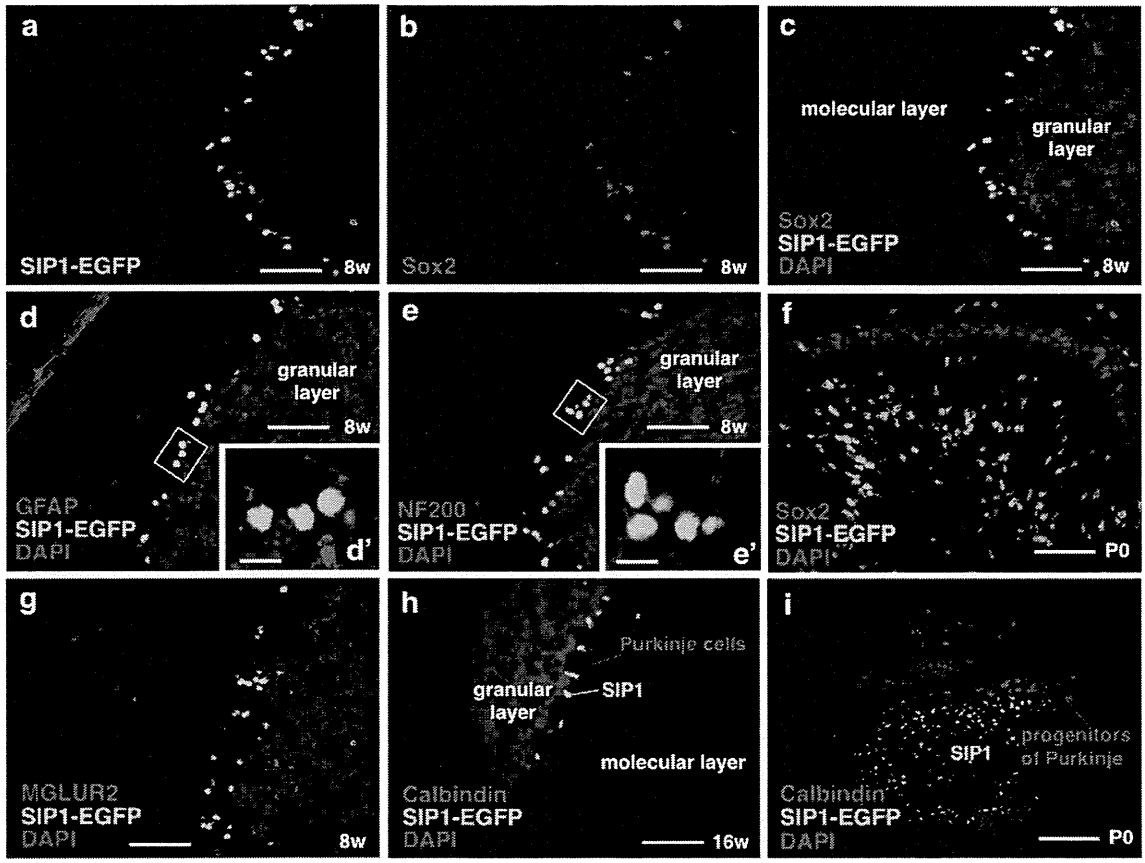

FIG. 5. Expression of SIP1-EGFP in Bergmann glial cells in the cerebellum. (**a–c**) Sagittal section of the 8w *Sip1*$^{SIP1\text{-}EGFP/+}$ mouse cerebellum immunostained with anti-GFP (green signal in a) and anti-Sox2 (red signal in b) antibodies. (c) is a merged image of (a) and (b) with DAPI counterstaining (blue). SIP1-EGFP expressing cells (green signals in a and c) located around the border between the molecular layer and granular layer (blue signal in c) were found to express a Bergmann glial marker, Sox2 (red signals in b and c). (**d, d′, e, e′**) Immunostained sagittal sections of the 8 week *Sip1*$^{SIP1\text{-}EGFP/+}$ mouse cerebellum with anti-glial fibrillary acidic protein (GFAP) antibodies (red signal in d and d′), anti-neurofilament 200 (NF 200) antibodies (red signal in e and e′), anti-GFP antibodies (green signal in d, d′, e, e′) and DAPI (blue signal in d, d′ and e, e′). (d′) and (e′) are higher magnification of the rectangular region of (d) and (e), respectively. It was observed also that most of the processes (red signals in d, d′, e, e′) of the SIP1-EGFP expressing cells (green signals in d, d′, e, e′) extended to the molecular layer, suggesting that they are unipolar neuroglial cells. (**g**) Immunostained sagittal section of the 8 week *Sip1*$^{SIP1\text{-}EGFP/+}$ mouse cerebellum with anti-metabotropic glutamate receptor 2 (MGLUR2) antibody (red), anti-GFP antibody (green), and DAPI (blue). The MGLUR2 expressing golgi cells (red) and SIP1 expressing cells (green) are different populations. (**h**) Immunostained coronal section of the 16w *Sip1*$^{SIP1\text{-}EGFP/+}$ mouse cerebellum with anti-Calbindin (red), anti-GFP (green) antibodies, and DAPI (blue). Calbindin-expressing Purkinje cells (red) were observed to be adjacent to the SIP1-EGFP expressing cells (green). (**f**) Sagittal section of the P0 *Sip1*$^{SIP1\text{-}EGFP/+}$ mouse cerebellum immunostained with anti-Sox2 antibody (red), anti-GFP antibody (green) and DAPI (blue). SIP1-EGFP positive cells expressed Sox2 at the cerebellar developing neonatal stage also. (**i**) Coronal section of the P0 *Sip1*$^{SIP1\text{-}EGFP/+}$ mouse cerebellum immunostained with anti-calbindin (red), anti-GFP (green) antibodies, and DAPI (blue). The SIP1-EGFP expressing cells were observed as a distinct population from the calbindin-positive Purkinje cell progenitors near the granular layer. Bars: 50 μm (a–h), 10 μm (d′ and e′) and 100 μm (i).

clones (#111 and #144) showed hybridization bands of the expected length. These clones were further analyzed and verified by Southern hybridization as correct homologs recombinants. Chimeric mice were generated by injecting these targeted ES cells into blastocysts as described previously (Higashi *et al.*, 2002). The male germ-line chimeric founders from the two independent ES cell lines (#111 and #144) were identified by the coat colors of the pups from crosses with C57BL/6N female mice. The loxP-flanked neomycin (neo) selection cassette introduced into intron 8 was finally removed by Cre recombinase-mediated excision via matings with Zp3-cre mice, which express the Cre recombinase exclusively in the growing oocyte during formation of the zona pellucida extra cellular glycoprotein (Lewandoski *et al.*, 1997). The SIP1-EGFP knock-in mouse strain described here will be available to the research community upon acceptance of this report for publication.

Mouse Husbandry and Genotyping

Mice were housed in environmentally controlled rooms of the animal facility of Institute for

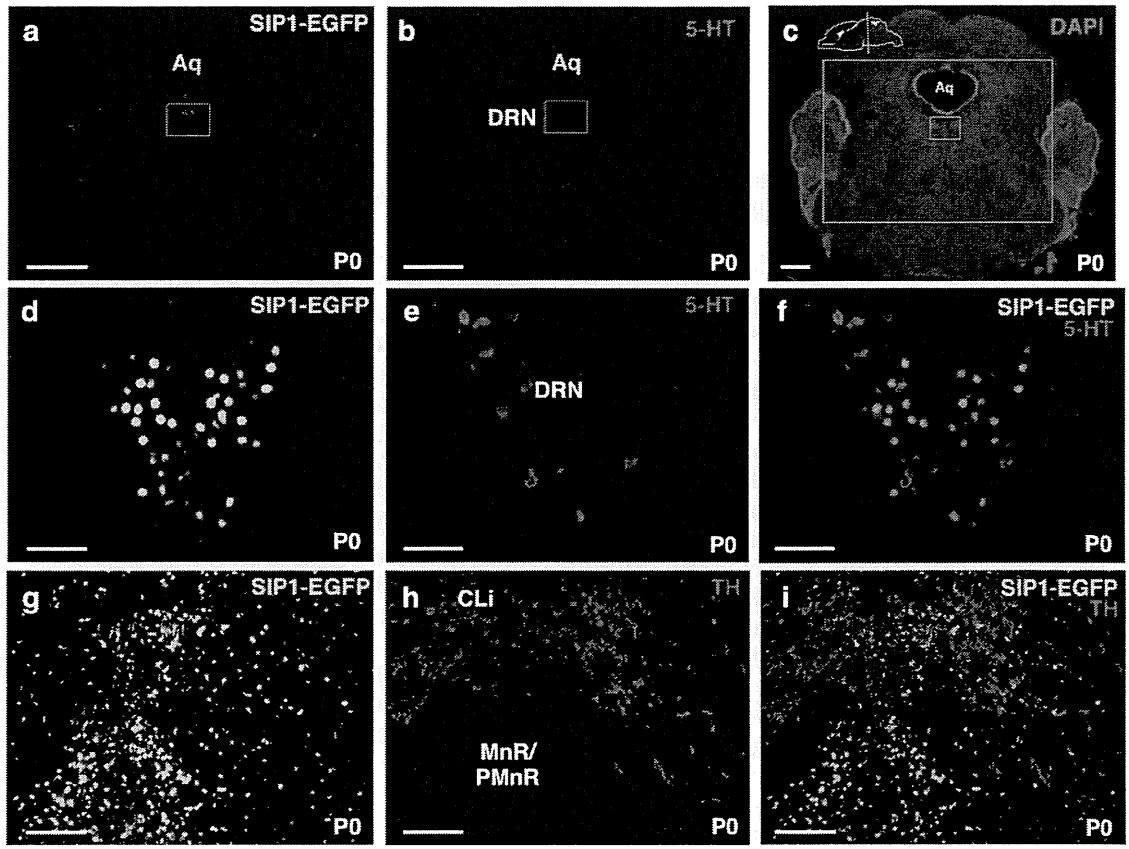

FIG. 6. Expression of SIP1-EGFP in the Raphe nucleus. (**a–c**) Coronal section of the P0 *Sip1*$^{SIP1\text{-}EGFP/+}$ mouse brainstem immunostained with anti-GFP (a), anti-serotonin (5-HT) (b) antibody and DAPI (c). (a and b) are high-magnification images of the larger rectangular region in (c). Bars: 500 μm. Diffuse and dispersed SIP1-EGFP expression is evident in the brainstem region and a small cluster of SIP1-EGFP expressing cells could be observed at the ventral side of the aqueduct (Aq) [rectangular region in (a)]. Serotonergic neurons are detectable as immunoreactive neurons against a 5-HT antibody on the ventral side of the aqueduct along the midline. The most dorsal area of the 5-HT positive region is the dorsal raphe nucleus (DRN) [rectangular area in (b)]. (**d–f**) Higher magnification of the small rectangular region in (a) and (b). Bars: 50 μm. (f) is a merged image of (d) and (e). The expression of SIP1-EGFP (green signal) could be observed in many of the anti-5-HT immunoreactive cells in the DRN (red signals). Intense 5-HT signal was observed in the cytoplasm and weak signal was found in the nuclei, whereas SIP1-EGFP expression was evident in the nuclei of the cells in the DRN. (**g–i**) Coronal section of the P0 *Sip1*$^{SIP1\text{-}EGFP/+}$ mouse brainstem immunostained with anti-GFP (g) and anti-tyrosine hydroxylase (TH) (h) antibodies. (i) is a merged image of (g) and (h). Some TH-positive dopaminergic neurons in the caudal linear nucleus of the raphe (CLi) were found to express SIP1-EGFP. The SIP1-EGFP expressing cells were observed also in the median raphe nucleus (MnR), and para-median raphe nucleus (PMnR) near the CLi. In the CLi cells, SIP1-EGFP expression was predominantly observed in the cellular nuclei but sometimes in the elongated cytoplasm. TH expression was observed in the cytoplasm of CLi cells. Bars: 100 μm.

Developmental Research (IDR), Aichi Human Service Center, Kasugai, Japan. All experiments were carried out in accordance with the protocols approved by the Animal Use Committee of IDR, and conformed also to the guidelines of the Japanese government for recombinant DNA experiments. Wild-type ICR mice for *in situ* hybridization were purchased from Japan SLC (Hamamatsu, Japan). *Sip1*$^{SIP1\text{-}EGFP/+}$ mice were crossed between littermates or with ICR mice after backcrossing for 2–5 generations onto the C57BL/6N strain. We noticed that the homozygous mice of the kock-in allele were viable under the mixed genetic background (e.g., hybrid between 129/sv and C57BL/6N, or C57BL/6N, and ICR strains), but they did not seem to survive after backcrossing into the inbred C57BL/6N strain, suggesting that the SIP1-EGFP fusion protein dose not work as perfectly as wild-type protein. Genotyping of wild-type and knock-in alleles was performed using genomic DNA extracts of ear punch tissue by PCR with the primers P1; 5′-GATGGGAAAATGGAAACCAAATCAGACCAC-3′ (*Sip1* allele forward primer), P2; 5′-TCGTGCTGCTTCA TGTGGTCGGGGTAGC-3′ (EGFP knock-in allele reverse primer), and P3; 5′-TTCTGTCCCTCTCTACAGCTTCC TGGAAGC-3′ (*Sip1* allele reverse primer). The amplification conditions were 94°C for 5 min, followed by 35 cycles of 94°C for 30 s, 64°C for 30 s 72°C for 1 min

and a final 72°C extension step for 7 min. The sizes of PCR amplicons from the wild-type and mutant alleles are 188 and 334 bp, respectively.

In Situ Hybridization

As the template for *in situ* probes, mouse *Sip1* full-length cDNA plasmid in pBluescriptII-KS was used (Miyoshi *et al.*, 2006; Van de Putte *et al.*, 2003). For digoxigenin (DIG) (Roche, Mannheim, Germany)-labeled riboprobes synthesization, *Sip1* cDNA containing plasmid were linearized with NotI for antisense and SalI for sense and transcribed using T3 or T7 polymerase for antisense or sense, respectively. Embryos were fixed with 4% paraformaldehyde (PFA) in phosphate buffered saline (PBS) for an overnight. Postnatal mice were prepared by perfusion-fixation with 4% PFA in PBS and then postfixed in 4% PFA in PBS for an overnight. Brains or whole embryos were embedded in paraffin and sectioned at 8 μm thickness. The sliced specimens were collected on the MAS coated glass slides (Matsunami, Osaka, Japan) and deparaffinizated with xylene. After rehydration and rinsing with PBS, the sections were treated with proteinase K (10 μg/ml) in PBS at room temperature for 5-10 min. After postfixation, the specimens were treated with 0.2*M* HCl for 10 min and then acetylated with 0.1*M* triethanolamine-HCl (pH 8.0)/0.25% acetic anhydrate for 10 min. The specimens were incubated with DIG-labeled riboprobe in hybridization solution (50% formamide (Promega, madison, WI), 10 m*M* Tris-HCl, pH 7.6, 200 μg/μl tRNA (Life Technologies, Carlsbad, CA), 1X Denhardt's solution, 10% dextran sulfate, 600 m*M* NaCl, 0.25% sodium dodecyl sulfate, 1 m*M* EDTA, pH 8.0) at 50°C for an overnight. After hybridization, sections were washed with 50% formamide/2× saline-sodium citrate (SSC) solution at 55°C for 30 min. To degrade unhybridized riboprobe, the sections were treated with RNaseA (10 μg/ml) (Wako, Osaka, Japan) in TNE (10 m*M* Tris-HCl, pH 7.5, 0.5*M* NaCl and 1 m*M* EDTA) at 37°C for 30 min. After washing with 2× SSC once and 0.2× SSC twice at 50°C for 20 min each, sections were washed and blocked with DIG wash and block buffer (Roche, Mannheim, Germany) and then immunoreacted to the alkaline phosphatase (AP)-conjugated anti-DIG antibody (1:1000; Roche, Mannheim, Germany) at room temperature for 1 h. Hybridization signals were visualized by BM purple AP substrate (Roche, Mannheim, Germany). After color detection, the sections were mounted with CC mount (DBS, Pleasanton, CA) mounting medium.

Immunohistochemistry

Adult mouse brains were prepared by perfusion-fixation with 4% PFA in PBS and then postfixed in 4% PFA in PBS for 4 h. Tissue from embryos was fixed with 4% PFA in PBS for 2-3 h. The embryos or brains were embedded in OCT compound (Sakura Finetek Japan, Tokyo, Japan) or Surgipath compound (Leica Biosystems, Nussloch, Germany) and frozen in liquid nitrogen. Frozen embedded compounds were sectioned at a thickness of 8 μm and collected onto glass slides. These cryosections were then washed three times with TBST (Tris buffered saline with 0.1% Tween 20) and treated with 10% normal goat serum or 2% bovine serum albumin (Sigma, St. Louis, MO) to block nonspecific binding. After 20 min incubation in this blocking solution at room temperature, the sections were incubated at 4°C overnight with antibodies against GFP (A11122, 1:250; Invitrogen, Carlsbad, CA; or GF090R, 1:500; Nacalai Tesque, Kyoto, Japan), Ctip2 (ab18465, 1:500; Abcam, Cambridge, England), Tbr1 (ab31940, 1:500; Abcam, Cambridge, England), Sox2 (ab97959, 1:1000; Abcam, Cambridge, England), NeuN (ab77315, 1:500; Abcam, Cambridge, England), APC (ab16794, 1:20; Abcam, Cambridge, England), calbindin D-28K (AB1778, 1:500; Millipore, Billerica, MA), neurofilament 200 (N4142, 1:500; Sigma, St. Louis, MO), MGLUR2 (SAB4501318, 1:100; Sigma, St. Louis, MO), GFAP (Z0334, 1:200; Daco), serotonin (S5545,1:1000; Sigma, St. Louis, MO), and tyrosine hydroxylase (MAB318, 1:200; Millipore, Billerica, MA). After washing, the specimens were incubated with fluorescent dye-conjugated secondary antibodies (Invitrogen, Carlsbad, CA) and 2 μg/μl 4′,6-Diamidino-2-phenylindole dihydrochloride (DAPI) (Sigma, St. Louis, MO) for 1 h. After washing, the specimens were mounted using Prolong Gold mounting medium (Invitrogen, Carlsbad, CA). In the case of staining for NeuN and APC, a mouse on mouse blocking kit and avidin biotin blocking kit (Vector, Burlingame, CA) were used to block the nonspecific binding of endogenous mouse IgG and biotin, respectively.

Fluorescence Image Acquisition and Processing

Images were acquired using an Olympus CCD camera DP70 mounted on a Nicon E800 microscope with DP controller (Olympus, Tokyo, Japan) software. The objective lenses used for image capture were Plan Apo 2×/NA0.1, Plan Fluor 4×/NA0.13, Plan Fluor 10×/NA0.30, Plan Fluor 20×/NA0.50, and Plan Fluor 40×/NA0.75. The filter sets used for excitation and emission wavelength of fluorescent dyes were as follows: 465-495 nm (excitation for green fluorescent) and 515-555 nm (emission for green fluorescent); 540-580 nm (excitation for red fluorescent), and 600-660 nm (emission for red fluorescent); 360-370 nm (excitation for DAPI) and 400 nm (emission for DAPI). Figures were processed and assembled using Photoshop, Pixelmator, ImageJ64, and PowerPoint software.

ACKNOWLEDGMENTS

The authors thank Dr. Takeshi Yagi (Osaka Univ. Osaka) for providing the pMC1-DT-ApA plasmid and Dr. Yoh

Wada (Osaka Univ. Osaka) for donating the pGPS21loxFRT-Neo plasmid. They are also grateful to Dr. Luc Nelles (KU Leuven, Leuven) for the SIP1 BAC clone (BAC 31209) and Dr. Neal G. Copeland (The Methodist Hospital Res. Inst. Houston) for the recombineering system. They also thank Dr. Keiko Nakanishi and Dr.Yoshihito Tokita in our laboratory for helpful discussions. The authors declare no conflicts of interest in relation to the work of this report.

LITERATURE CITED

Aoyama M, Agari K, Sun-Wada GH, Futai M, Wada Y. 2005. Simple and straightforward construction of a mouse gene targeting vector using in vitro transposition reactions. Nucleic Acids Res 33:e52.

Arlotta P, Molyneaux BJ, Chen J, Inoue J, Kominami R, Macklis JD. 2005. Neuronal subtype-specific genes that control corticospinal motor neuron development in vivo. Neuron 45:207-221.

Bhat RV, Axt KJ, Fosnaugh JS, Smith KJ, Johnson KA, Hill DE, Kinzler KW, Baraban JM. 1996. Expression of the APC tumor suppressor protein in oligodendroglia. Glia 17:169-174.

Brill MS, Ninkovic J, Winpenny E, Hodge RD, Ozen I, Yang R, Lepier A, Gascon S, Erdelyi F, Szabo G, Parras C, Guillemot F, Frotscher M, Berninger B, Hevner RF, Raineteau O, Gotz M. 2009. Adult generation of glutamatergic olfactory bulb interneurons. Nat Neurosci 12:1524-1533.

Doetsch F, Garcia-Verdugo JM, Alvarez-Buylla A. 1997. Cellular composition and three-dimensional organization of the subventricular germinal zone in the adult mammalian brain. J Neurosci 17:5046-5061.

Hatten ME, Alder J, Zimmerman K, Heintz N. 1997. Genes involved in cerebellar cell specification and differentiation. Curr Opin Neurobiol 7:40-47.

Higashi Y, Maruhashi M, Nelles L, Van de Putte T, Verschueren K, Miyoshi T, Yoshimoto A, Kondoh H, Huylebroeck D. 2002. Generation of the floxed allele of the SIP1 (Smad-interacting protein 1) gene for Cre-mediated conditional knockout in the mouse. Genesis 32:82-84.

Lewandoski M, Wassarman KM, Martin GR. 1997. Zp3-cre, a transgenic mouse line for the activation or inactivation of loxP-flanked target genes specifically in the female germ line. Curr Biol 7:148-151.

Liu P, Jenkins NA, Copeland NG. 2003. A highly efficient recombineering-based method for generating conditional knockout mutations. Genome Res 13:476-484.

McKenna WL, Betancourt J, Larkin KA, Abrams B, Guo C, Rubenstein JL, Chen B. 2011. Tbr1 and Fezf2 regulate alternate corticofugal neuronal identities during neocortical development. J Neurosci 31:549-564.

McKinsey GL, Lindtner S, Trzcinski B, Visel A, Pennacchio LA, Huylebroeck D, Higashi Y, Rubenstein JL. 2013. Dlx1&2-dependent expression of Zfhx1b (Sip1, Zeb2) regulates the fate switch between cortical and striatal interneurons. Neuron 77:83-98.

Miquelajauregui A, Van de Putte T, Polyakov A, Nityanandam A, Boppana S, Seuntjens E, Karabinos A, Higashi Y, Huylebroeck D, Tarabykin V. 2007. Smad-interacting protein-1 (Zfhx1b) acts upstream of Wnt signaling in the mouse hippocampus and controls its formation. Proc Natl Acad Sci U S A 104: 12919-12924.

Miyoshi T, Maruhashi M, Van De Putte T, Kondoh H, Huylebroeck D, Higashi Y. 2006. Complementary expression pattern of Zfhx1 genes Sip1 and deltaEF1 in the mouse embryo and their genetic interaction revealed by compound mutants. Dev Dyn 235:1941-1952.

Nagy A, Rossant J, Nagy R, Abramow-Newerly W, Roder JC. 1993. Derivation of completely cell culture-derived mice from early-passage embryonic stem cells. Proc Natl Acad Sci U S A 90:8424-8428.

Nelles L, Van de Putte T, van Grunsven L, Huylebroeck D, Verschueren K. 2003. Organization of the mouse Zfhx1b gene encoding the two-handed zinc finger repressor Smad-interacting protein-1. Genomics 82: 460-469.

Nityanandam A, Parthasarathy S, Tarabykin V. 2012. Postnatal subventricular zone of the neocortex contributes GFAP+ cells to the rostral migratory stream under the control of Sip1. Dev Biol 366:341-356.

Ohishi H, Shigemoto R, Nakanishi S, Mizuno N. 1993. Distribution of the messenger RNA for a metabotropic glutamate receptor, mGluR2, in the central nervous system of the rat. Neuroscience 53:1009-1018.

Seuntjens E, Nityanandam A, Miquelajauregui A, Debruyn J, Stryjewska A, Goebbels S, Nave KA, Huylebroeck D, Tarabykin V. 2009. Sip1 regulates sequential fate decisions by feedback signaling from postmitotic neurons to progenitors. Nat Neurosci 12:1373-1380.

Sottile V, Li M, Scotting PJ. 2006. Stem cell marker expression in the Bergmann glia population of the adult mouse brain. Brain Res 1099:8-17.

Van de Putte T, Francis A, Nelles L, van Grunsven LA, Huylebroeck D. 2007. Neural crest-specific removal of Zfhx1b in mouse leads to a wide range of neurocristopathies reminiscent of Mowat-Wilson syndrome. Hum Mol Genet 16:1423-1436.

Van de Putte T, Maruhashi M, Francis A, Nelles L, Kondoh H, Huylebroeck D, Higashi Y. 2003. Mice lacking ZFHX1B, the gene that codes for Smad-interacting protein-1, reveal a role for multiple neural crest cell defects in the etiology of Hirschsprung

disease-mental retardation syndrome. Am J Hum Genet 72:465-470.

van den Berghe V, Stappers E, Vandesande B, Dimidschstein J, Kroes R, Francis A, Conidi A, Lesage F, Dries R, Cazzola S, Berx G, Kessaris N, Vanderhaeghen P, van Ijcken W, Grosveld FG, Goossens S, Haigh JJ, Fishell G, Goffinet A, Aerts S, Huylebroeck D, Seuntjens E. 2013. Directed migration of cortical interneurons depends on the cell-autonomous action of Sip1. Neuron 77: 70-82.

van Grunsven LA, Michiels C, Van de Putte T, Nelles L, Wuytens G, Verschueren K, Huylebroeck D. 2003. Interaction between Smad-interacting protein-1 and the corepressor C-terminal binding protein is dispensable for transcriptional repression of E-cadherin. J Biol Chem 278:26135-26145.

Verschueren K, Remacle JE, Collart C, Kraft H, Baker BS, Tylzanowski P, Nelles L, Wuytens G, Su MT, Bodmer R, Smith JC, Huylebroeck D. 1999. SIP1, a novel zinc finger/homeodomain repressor, interacts with Smad proteins and binds to 5'-CACCT sequences in candidate target genes. J Biol Chem 274:20489-20498.

Wakamatsu N, Yamada Y, Yamada K, Ono T, Nomura N, Taniguchi H, Kitoh H, Mutoh N, Yamanaka T, Mushiake K, Kato K, Sonta S, Nagaya M. 2001. Mutations in SIP1, encoding Smad interacting protein-1, cause a form of Hirschsprung disease. Nat Genet 27:369-370.

Weng Q, Chen Y, Wang H, Xu X, Yang B, He Q, Shou W, Chen Y, Higashi Y, van den Berghe V, Seuntjens E, Kernie SG, Bukshpun P, Sherr EH, Huylebroeck D, Lu QR. 2012. Dual-mode modulation of Smad signaling by Smad-interacting protein Sip1 is required for myelination in the central nervous system. Neuron 73:713-728.

Yaguchi J, Angerer LM, Inaba K, Yaguchi S. 2012. Zinc finger homeobox is required for the differentiation of serotonergic neurons in the sea urchin embryo. Dev Biol 363:74-83.

Yamada K, Watanabe M. 2002. Cytodifferentiation of Bergmann glia and its relationship with Purkinje cells. Anat Sci Int 77:94-108.

Yanagawa Y, Kobayashi T, Ohnishi M, Kobayashi T, Tamura S, Tsuzuki T, Sanbo M, Yagi T, Tashiro F, Miyazaki J. 1999. Enrichment and efficient screening of ES cells containing a targeted mutation: The use of DT-A gene with the polyadenylation signal as a negative selection maker. Transgenic Res 8:215-221.

厚生労働科学研究費補助金

障害者対策総合研究事業（神経・筋疾患分野）

下部神経管閉鎖障害の病態・制御研究

平成25年度　総括・分担研究報告書

発行　　平成26年5月

発行所　下部神経管閉鎖障害の病態・制御研究班事務局

名古屋大学大学院医学系研究科神経遺伝情報学分野

〒466-8550　名古屋市昭和区鶴舞町65

TEL: 052-744-2447　FAX: 052-744-2449